International Journal of Heat and Mass Transfer 53 (2010) 2969–2978

Contents lists available at ScienceDirect

International Journal of Heat and Mass Transfer

journal homepage: www.elsevier.com/locate/ijhmt

Phase-field modeling of bubble growth and flow in a Hele–Shaw cell

Y. Sun [a], C. Beckermann [b,*]

[a] Department of Mechanical Engineering and Mechanics, Drexel University, Philadelphia, PA 19104, USA
[b] Department of Mechanical and Industrial Engineering, The University of Iowa, Iowa City, IA 52242, USA

ARTICLE INFO

Article history:
Received 20 October 2009
Received in revised form 11 March 2010
Accepted 11 March 2010
Available online 18 April 2010

Keywords:
Phase-field method
Two-phase flows
Bubble growth

ABSTRACT

A phase-field model is presented for gas bubble growth and flow in a supersaturated liquid inside a Hele–Shaw cell. The flows in the gas and liquid are solved using a two-phase diffuse interface model that accounts for surface tension, interfacial mass transfer, and density and viscosity differences between the phases. This model is coupled with a phase-field equation for interface motion and a diffuse interface conservation equation for gas species transport. The model is first validated for a planar gas layer and a spherical bubble growing in a supersaturated liquid. It is shown that the results converge to the solution of the corresponding sharp interface model in the thin-interface limit. The model capabilities are demonstrated in several examples involving the growth and flow of multiple bubbles, including bubble coarsening and coalescence.

1. Introduction

Gas bubble growth in a liquid is an important phenomenon in materials processing, biological systems, oil recovery, and other applications. The liquid can become supersaturated in a gas species due to a drop in pressure or temperature. Pre-existing or newly nucleated bubbles then grow by diffusion of the gas species in the liquid towards the bubble interface. The large density difference between the liquid and the gas induces an expansion flow in the liquid during bubble growth. The growth of a single stationary spherical gas bubble has been investigated in detail [1–4]. In reality, the bubble shape during growth is not always spherical, especially if the bubble interacts with a solid boundary or moves in a viscous liquid. Furthermore, pinch-off and coalescence of multiple bubbles can cause interface topology changes. The motion of multiple bubbles in a liquid has been simulated using a variety of models and numerical methods (see, for example, [5–8]). However, no studies have been identified in the literature where the growth and flow of gas bubbles, including interface topology changes, is simulated simultaneously.

Two-phase flows featuring topology transitions and other interface singularities have become an area of increasing research interest over the last decade [9–14]. In such flows, multiple length and time scales emerge, and capillary stresses cannot be neglected. For the nano-scale phenomena introduced by interface singularities, conventional sharp interface models fail to work [10,11]. Diffuse interface approaches have been proposed to overcome these difficulties [9,12–18]. In diffuse interface models, the interface is viewed as a region of finite extent over which the properties vary smoothly from one phase to the other. The main objective of the present study is to present and test a diffuse interface model for the growth and flow of gas bubbles in a liquid. A diffuse interface model for such a system has not been developed previously.

All thermodynamically derived diffuse interface models for fluid flow [9,12–14,17] assume the existence of a single velocity and pressure at any point inside the diffuse interface between two phases. Moreover, single thermo-physical properties (e.g., density and viscosity) are assumed to exist and their variation across the diffuse interface is postulated in some ad hoc manner. For large differences in these properties between the phases, such diffuse interface models can give results that are dependent on the choice of the interface width [16] and the way the property variations are specified [17]. Based on an ensemble averaging approach, Sun and Beckermann [16] developed a so-called two-phase diffuse interface model for flow. As opposed to thermodynamically derived diffuse interface models, the two phases are assumed to coexist inside the diffuse interface with different properties, velocities, and pressures. The phase interactions are modeled explicitly through the inclusion of interfacial forces in the momentum equations for each phase. Capillary stresses inside the diffuse interface are included in the model as well. One unique feature of the model is that for simple shear flows, the results are independent of the diffuse interface width. This allows for the use of artificially large interface widths in numerical simulations and, hence, significantly improves computational efficiency.

In the present study, the two-phase diffuse interface model of Ref. [16] is applied to simulate the flow of the gas and liquid phases during bubble growth inside a Hele–Shaw cell. Compared to a full Navier–Stokes formulation, the Hele–Shaw approximation allows

* Corresponding author. Tel.: +1 (319) 335 5681; fax: +1 (319) 335 5669.
E-mail address: becker@engineering.uiowa.edu (C. Beckermann).

0017-9310/$ - see front matter © 2010 Elsevier Ltd. All rights reserved.
doi:10.1016/j.ijheatmasstransfer.2010.03.036

Nomenclature

a_1, a_2	constants in the phase-field model
b	gap width in the Hele–Shaw cell
C	concentration
D	mass diffusivity
$\widetilde{D}$	dimensionless mass diffusivity
d_0	capillary length
K_s	equilibrium constant in Sieverts' law
L	length of the Hele–Shaw cell
$\boldsymbol{n}$	unit normal vector
p	pressure
R	gas constant
r_ρ	density ratio
r_μ	viscosity ratio
T	temperature
t	time
U	dimensionless concentration
$\boldsymbol{u}$	velocity vector
$\boldsymbol{u}_i$	interface velocity vector
V	interface velocity
W	measure of diffuse interface width
x	space coordinate

Greek symbols

δ	width of planar gas layer
ε	measure of diffuse interface width
ϕ	phase field
Γ	mass transfer rate per unit volume
κ	mean interface curvature
λ	coupling constant
μ	viscosity
ρ	density
σ	surface tension
τ	dimensionless time

Superscripts

$'$	dimensionless
0	reference

Subscripts

eq	equilibrium
g	gas
i	interface
k	phase k
l	liquid
n	interface normal direction
ref	reference
0	reference
∞	far field

for two-dimensional simulations to be performed at a much reduced computational cost. A two-phase diffuse interface Hele–Shaw model was recently applied by the present authors to simulate flows where the two phases have a large contrast in the density and viscosity [19]. This model is extended here to include interfacial mass transfer due to bubble growth. During bubble growth, the gas–liquid interface is assumed to be in equilibrium and the dissolved gas concentration on the liquid side of the interface is related to the gas pressure by Sieverts' law. The present study focuses on bubbles of a diatomic gas in a liquid metal (in particular, Al–H), although the model is easily modified for other gas–liquid combinations. Sieverts' law is valid for dissociative dissolution, when diatomic gases such as O_2, N_2, or H_2 enter metals (M) to form M–O, M–N, or M–H bonds [20,21]. The phase-field equation is derived using a thin-interface approach [22,23]. It reduces to the Gibbs–Thomson condition for a sharp gas–liquid interface when the diffuse interface width is still finite, while eliminating interface kinetic effects. The phase-field equation is valid in the presence of flow and density changes of the gas. The diffuse interface species conservation equation accounts for diffusion and advection of the gas species in the liquid. It includes an anti-trapping current analogous to that developed by Karma [22] for unequal diffusivities in the phases. The resulting model allows for quantitative simulation of bubble growth and flow in a numerically efficient manner.

The governing equations are presented in Section 2. In Section 3, the model is tested by applying it to two simple problems that allow for detailed convergence studies and a comparison with an analytical solution. More complex examples demonstrating the utility of the present model, including coarsening of multiple bubbles in a liquid and bubble growth and flow with interface topology changes, are presented in Section 4. The conclusions are summarized in Section 5.

2. Governing equations

In this section, the two-phase diffuse interface model for bubble growth and flow in a Hele–Shaw cell is presented. First, the traditional sharp interface formulation of the problem is stated. Then, the diffuse interface model for two-phase flows of the present authors [16,19] is extended to include bubble growth and mass transfer. A phase-field equation for the evolution of the gas–liquid interface is constructed in a similar fashion as the quantitative phase-field model of Karma [22] for isothermal alloy solidification. Finally, a conservation equation is presented for the advection-diffusion of the gas species, including an anti-trapping current analogous to that of Karma [22].

2.1. Sharp interface description

Consider bubbles of a diatomic gas (i.e., H_2) surrounded by a liquid metal (i.e., Al) inside a Hele–Shaw cell. The liquid is a binary mixture with the (nonvolatile) metal (Al) as the solvent and the gas species (H) as the solute. The system is taken as isothermal and the mass diffusivity of the gas species in the liquid is assumed to be constant. Equilibrium at the gas–liquid interface is governed by Sieverts' law.

The liquid surrounding the bubbles is assumed to be an incompressible Newtonian fluid with constant viscosity and density. Gravitational effects are neglected (i.e., the Hele–Shaw cell is horizontal). Initially, the liquid is assumed to be at rest, having a uniform solute concentration C_∞ and pressure p_{ref}. The Hele–Shaw cell has a gap of width b that is much smaller than the cell length or width, L (i.e., $b \ll L$). Assuming a parabolic velocity profile in the gap direction, the sharp interface description of this problem is given by:

Liquid

$$\nabla \cdot \boldsymbol{u}_l = 0 \quad \text{(continuity)} \tag{1}$$

$$\boldsymbol{u}_l = -\frac{b^2}{12\mu_l}\nabla p_l \quad \text{(momentum)} \tag{2}$$

$$\frac{\partial C_l}{\partial t} + \boldsymbol{u}_l \cdot \nabla C_l = D\nabla^2 C_l \quad \text{(species)} \tag{3}$$

Gas

$$\frac{\partial \rho_g}{\partial t} + \nabla \cdot (\rho_g \boldsymbol{u}_g) = 0 \quad \text{(continuity)} \tag{4}$$

$$\boldsymbol{u}_g = -\frac{b^2}{12\mu_g}\nabla p_g \quad \text{(momentum)} \tag{5}$$

$$p_g = \rho_g RT \quad \text{(ideal gas law)} \tag{6}$$

Interface

$$\|\rho(\boldsymbol{u} - \boldsymbol{u}_i)\cdot \boldsymbol{n}\| = 0 \quad \text{(continuity)} \tag{7}$$

$$p_g - p_l = \sigma\kappa \quad \text{(momentum)} \tag{8}$$

$$\|\rho C(\boldsymbol{u} - \boldsymbol{u}_i)\cdot \boldsymbol{n} - \rho D\nabla C \cdot \boldsymbol{n}\| = 0 \quad \text{(species)} \tag{9}$$

$$C_{l,i} = C_{eq}(T, p_g)\left(1 + \frac{\sigma\kappa}{\rho_l RT}\right) \quad \text{(Gibbs—Thomson)} \tag{10}$$

The various symbols are defined in the Nomenclature. The symbol $\| \ \|$ denotes a jump across the interface of a function f as $\|f\| = f_g - f_l$. A species conservation equation for the gas phase is not needed, since the bubbles are assumed to consist of a single component, i.e., $C_g = 1$. The last term in the Gibbs–Thomson equation, Eq. (10), accounts for the effect of interface curvature on the equilibrium concentration in the liquid at the gas–liquid interface [20,21]. The equilibrium concentration for a planar interface is obtained from Sieverts' law

$$C_{eq} = K_s\sqrt{\frac{p_g}{p_{ref}}} \tag{11}$$

where the reference pressure is taken as atmospheric pressure. For hydrogen in liquid aluminum, the equilibrium constant, K_s, is given by [21]

$$K_s = 8.9 \times 10^{-5} \times 10^{-\frac{2760}{T}+2.796} \tag{12}$$

2.2. Diffuse interface description

2.2.1. Continuity and momentum equations

The diffuse interface continuity and momentum equations are obtained from the two-phase model of Sun and Beckermann [16]. For Hele–Shaw flows, the equations in Ref. [16] are averaged across the gap width, b, and scaled under the assumption that $b \ll L$ [19]. The resulting continuity equation for phase k is given by [19]

$$\frac{\partial \phi_k \rho_k}{\partial t} + \nabla \cdot (\phi_k \rho_k \boldsymbol{u}_k) = \Gamma_k \tag{13}$$

where k = g, l. The liquid density is assumed to be constant, whereas the density of the gas is calculated from the ideal gas law, Eq. (6). The phase-field variable, $\phi = \phi_g = 1 - \phi_l$, can be interpreted as a volume fraction. It varies in a hyperbolic tangent fashion across the diffuse interface of thickness 6ε [16,19] and takes on constant values of $\phi = 1$ and $\phi = 0$ inside the gas and liquid phases, respectively. The interfacial mass fluxes due to bubble growth, Γ_k, are balanced according to

$$\Gamma_g = -\Gamma_l \tag{14}$$

The diffuse interface version of the momentum equation for phase k is given by [19]

$$\boldsymbol{u}_k = -\frac{b^2}{12\mu_k}\left[\nabla p_k + \sigma\varepsilon(1-\phi_k)\nabla\left(\frac{\nabla^2\phi_k}{\phi_k(1-\phi_k)}\right)\right] \tag{15}$$

The second term inside the square brackets of Eq. (15) is the capillary stress gradient in phase k and is non-zero only inside the diffuse interface. The derivation and a detailed examination of this term can be found in Refs. [16,19]. Finally, the diffuse interface version of the interfacial momentum balance is given by [19]

$$p_g - p_l = -\sigma\varepsilon\frac{\nabla^2\phi}{\phi(1-\phi)} \tag{16}$$

The above continuity and momentum equations are valid in the entire domain, regardless of the phase present. They are solved using a procedure similar to that in Ref. [19]. The equations are combined and re-written in terms of a mixture density $\rho = \rho_g\phi + \rho_l(1-\phi)$, a mixture velocity $\boldsymbol{u} = [\rho_g\phi\boldsymbol{u}_g + \rho_l(1-\phi)\boldsymbol{u}_l]/\rho$, a slip velocity $\Delta\boldsymbol{u} = \boldsymbol{u}_g - \boldsymbol{u}_l$, and a mixture pressure $p = p_g\phi + p_l(1-\phi)$. Then, the mixture continuity and momentum equations are combined to form a Poisson equation for the mixture pressure, which can be solved numerically using a standard finite-difference method [19]. Before solving the continuity and momentum equations, they are non-dimensionalized using the length and time scales introduced in the next section.

2.2.2. Phase-field equation

The phase-field equation for bubble growth and motion is derived using the thin-interface method explained in Ref. [18] and is similar to the one for binary alloy solidification in Refs. [22–24]. The final result is given in dimensionless form by

$$\left(C_g' - C_l'\right)\Gamma_g' = \nabla'^2\phi - 2\phi(1-\phi)(1-2\phi) + 8\lambda\left(C_l' - K_s'(T)\sqrt{p_g'}\right)\phi^2(1-\phi)^2 \tag{17}$$

In Eq. (17), the interfacial mass transfer rate due to bubble growth, Γ_g', is obtained from the continuity equation for the gas phase, Eq. (13) with k = g. In dimensionless form, it can be written as

$$\Gamma_g' = \frac{\partial(r_\rho\phi)}{\partial t'} + \nabla'\cdot(r_\rho\phi\boldsymbol{u}_g') \tag{18}$$

where $\boldsymbol{u}_g' = \boldsymbol{u}_g\tau_0/W$ is the dimensionless gas velocity and $r_\rho = \rho_g/\rho_l$ is the (variable) density ratio. The dimensionless concentrations are defined as $C_l' = C_l/C_{eq}^0$ and $C_g' = C_g/C_{eq}^0$ (recall that $C_g = 1$), where $C_{eq}^0 = C_{eq}(T_0, p_{ref}) = K_s(T_0)$ is the equilibrium concentration for a planar interface at the system reference temperature T_0. The dimensionless equilibrium coefficient is given by $K_s' = K_s/C_{eq}^0$ and the dimensionless gas pressure by $p_g' = p_g/p_{ref}$. Note that by using Eq. (18) for the interfacial mass transfer rate, Γ_g', the phase-field equation is valid in the presence of flow and density changes of the gas.

The length and time scales used to non-dimensionalize the phase-field equation are $W = \sqrt{2}\varepsilon$ and $\tau_0 = \left(d_0^2/D\right)a_2\lambda^3/a_1^2$, respectively. The capillary length is given by $d_0 = \sigma/(\rho_l RT_0)$ and the coupling constant between the phase field and the concentration field is given by $\lambda = a_1W/d_0$. Following the thin-interface analyses in Refs. [22–25], $a_1 = 5/\left(4\sqrt{2}\right)$ for the present choice of functions. In order to model kinetics-free bubble growth, $a_2 = D'/\lambda$, where the dimensionless diffusivity is given by $D' = D\tau_0/W^2$. The coupling constant λ is the only free parameter and the results should be independent of λ when they are converged. Decreasing λ corresponds to decreasing the diffuse interface width. When simulations are performed for different values of λ, the time and length scales vary with λ. Therefore, the results must be converted back to physical units before comparing them. It is emphasized again that this relatively complex prescription stems directly from the thin-interface analysis developed previously for binary alloy solidification [22–24], and the reader is referred to these references for a detailed derivation of the phase-field equation.

2.2.3. Species equation

The diffuse interface version of the conservation equation for the gas species is derived using the two-phase averaging method described in Sun and Beckermann [16]. It has been shown [15,24,26] that the species equation derived using the two-phase

averaging method is identical to the one derived from a variational formulation [22,24]. The dimensionless form of the diffuse interface species equation is given by

$$(1-\phi)\frac{\partial C_l'}{\partial t'} + (1-\phi)\boldsymbol{u}_l' \cdot \nabla' C_l' = \nabla' \cdot \left[D'(1-\phi)\nabla' C_l' - \frac{1}{\sqrt{2}}\left(C_g' - C_l'\right)\Gamma_g' \frac{\nabla'\phi}{|\nabla'\phi|}\right] - \left(C_g' - C_l'\right)\Gamma_g' \tag{19}$$

The second term in the square parenthesis on the right-hand-side of Eq. (19) is the so-called anti-trapping current due to Karma [22]. The anti-trapping current does not arise from averaging, but is introduced to recover local equilibrium at the gas–liquid interface and eliminate spurious effects that arise for a finite interface width when the diffusivities are unequal in the gas and liquid. Eq. (19) is similar to the species equation used in phase-field modeling of alloy solidification [22,24], but the effects of liquid and gas flow are taken into account. The gas velocity comes into Eq. (19) through the term involving Γ_g' [see Eq. (18)]. The above species equation is valid regardless of the phase present (i.e., even in the limit of $\phi \to 1$), and is solved over the entire domain.

3. Model validation

The present phase-field model is first validated for two relatively simple problems. In the first problem, the model is compared to an analytical sharp interface solution for a planar gas layer growing into a supersaturated liquid under purely diffusive conditions. The second problem involves the growth of a spherical bubble in a supersaturated, infinite liquid and includes the flow in the liquid due to the density difference between the gas and the liquid. This problem is used to demonstrate convergence of the results with respect to the diffuse interface width. It is important to note that the flow part of the present model, excluding interfacial mass transfer, was already validated in Ref. [19]. In particular, it is demonstrated in that reference that the present two-phase approach shows good convergence properties with respect to the diffuse interface width, even for large property (density and viscosity) contrasts between the phases.

3.1. Growth of a planar gas layer in a supersaturated liquid

Consider the propagation of a planar gas–liquid front in a supersaturated liquid of initial hydrogen concentration C_∞. As illustrated in Fig. 1, the gas layer has a thickness of $\delta(t)$ and the gas–liquid interface moves along the x-axis due to diffusion of hydrogen through the liquid toward the interface. The entire system is at a uniform temperature equal to T_0. The effect of the expansion flow in the liquid on the growth of the gas layer is neglected, which is a reasonable assumption for small density ratios and/or low interface velocities. The pressure is assumed constant at p_{ref}, which is equal to atmospheric pressure. The sharp interface description of this problem consists of the following diffusion equation inside the liquid:

$$\frac{\partial C}{\partial t} = D\frac{\partial^2 C}{\partial x^2} \quad \text{for } x \geqslant \delta \tag{20}$$

and the following boundary conditions at the gas–liquid interface:

$$(1-C_{eq})V = D\left.\frac{\partial C}{\partial x}\right|_l \quad \text{at } x = \delta \tag{21}$$

$$C = C_{eq} \quad \text{at } x = \delta \tag{22}$$

$$C = C_\infty \quad \text{at } x \to \infty \tag{23}$$

where V is the normal velocity of the gas–liquid interface. The initial condition is given by

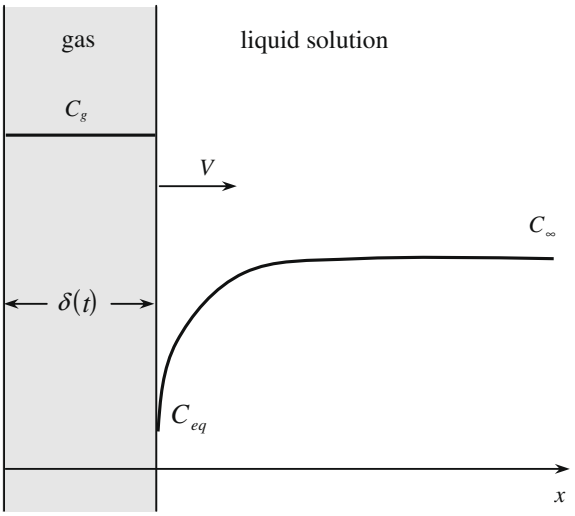

Fig. 1. Growth of a gas layer in a supersaturated liquid.

$$C = C_\infty \quad \text{for } t = 0 \quad \text{and} \quad x \geqslant \delta \tag{24}$$

Defining a dimensionless supersaturation as $U = (C_l - C_{eq})/(1 - C_{eq})$, Eqs. (20)–(24) can be re-written as

$$\frac{\partial U}{\partial t} = D\frac{\partial^2 U}{\partial x^2} \quad \text{for } x \geqslant \delta \tag{25}$$

$$V = D\left.\frac{\partial U}{\partial x}\right|_l \quad \text{at } x = \delta \tag{26}$$

$$U = 0 \quad \text{at } x = \delta \tag{27}$$

$$U = U_\infty \ (U_\infty > 0) \quad \text{at } x \to \infty \tag{28}$$

$$U = U_\infty \quad \text{for } t = 0 \quad \text{and} \quad x \geqslant \delta \tag{29}$$

The exact solution to this problem is time-dependent and is given by

$$U = U_\infty \mathrm{erf}\left(\frac{x-\delta}{2\sqrt{Dt}}\right) \tag{30}$$

$$V = U_\infty\sqrt{\frac{D}{\pi t}} \tag{31}$$

$$\delta = 2U_\infty\sqrt{\frac{Dt}{\pi}} \tag{32}$$

where erf(x) is the error function.

The phase-field and diffuse interface species equations for this problem can be obtained by simplifying Eqs. (17) and (19). In terms of the dimensionless concentration U, the result is given by

$$(1-U)\frac{\partial\phi}{\partial t'} = \frac{\partial^2\phi}{\partial x'^2} - 2\phi(1-\phi)(1-2\phi) + 8\lambda\phi^2(1-\phi)^2 U \tag{33}$$

$$\frac{\partial U}{\partial t'} = \frac{\partial}{\partial x'}\left[D'(1-\phi)\frac{\partial U}{\partial x'} + \frac{1}{\sqrt{2}}(1-U)\frac{\partial\phi}{\partial t'}\right] - \frac{\partial}{\partial t'}[\phi(1-U)] \tag{34}$$

since $\nabla'\phi/|\nabla'\phi| = -1$ for the present problem. Eqs. (33) and (34) are solved numerically using a standard second-order explicit finite-difference method. The results are converted back to physical units using the properties listed in Table 1.

Fig. 2 shows the predicted gas–liquid interface velocity, Vd_0/D, as a function of the coupling constant, λ, at a dimensionless time of $Dt/d_0^2 = 20,535$, for $U_\infty = 0.1$. Recall that decreasing λ corresponds to decreasing the diffuse interface width, since $\lambda = a_1 W/d_0$. The results in this figure are for a grid spacing of $\Delta x/W = 0.4$ and a time step of $\Delta t/\tau_0 = 0.008$. It can be seen that the results from the phase-field model converge to the exact solution for $\lambda \leqslant 4$. Unless otherwise noted, $\lambda = 4$ is used in the following. The conver-

Table 1
Parameters and properties used in the simulations of hydrogen gas bubble growth in a supersaturated aluminum melt.

Parameter	Symbol	Value
Initial hydrogen equilibrium concentration	C_{eq}^0	5×10^{-5} wt%
Far-field hydrogen concentration	C_∞	6×10^{-5} wt%
Hydrogen diffusion coefficient	D	3×10^{-7} m^2/s
Initial gas–liquid density ratio	r_ρ^0	0.00001
Gas–liquid viscosity ratio	r_μ	0.01
Chemical capillary length	d_0	1.14×10^{-3} μm
Liquid density	ρ_l	2390 kg/m^3
Liquid viscosity	μ_l	4.5×10^{-3} N/(m^2 s)
Surface tension	σ	0.8 N/m

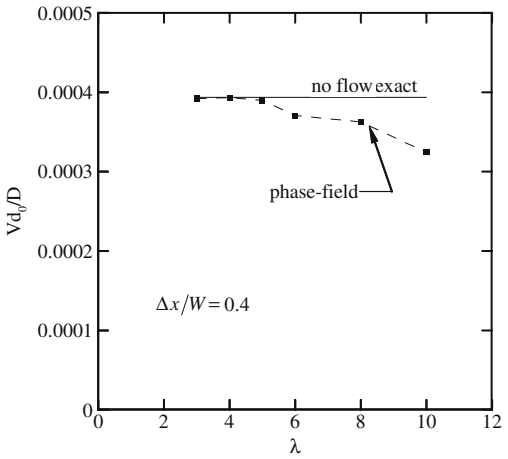

Fig. 2. Convergence of the interface velocity with respect to the diffuse interface coupling constant λ for growth of a planar gas layer in a supersaturated liquid $\left(Dt/d_0^2 = 20,535\right)$.

gence of the results with respect to the grid spacing, $\Delta x/W$, is examined in Fig. 3 (again for $U_\infty = 0.1$ at $Dt/d_0^2 = 20,535$). The phase-field model results agree well with the analytical solution for all $\Delta x/W \leqslant 1$. In order to ensure good accuracy, a value of $\Delta x/W = 0.4$ is used in all subsequent phase-field simulations.

Transient solutions of the phase-field model are presented in Fig. 4. Fig. 4a shows the evolution of the dimensionless supersaturation, U, in the liquid, every 20,000 time steps, for $U_\infty = 0.1$. As expected, the diffusion boundary layer ahead of the gas–liquid interface becomes thicker as time progresses. The predicted time

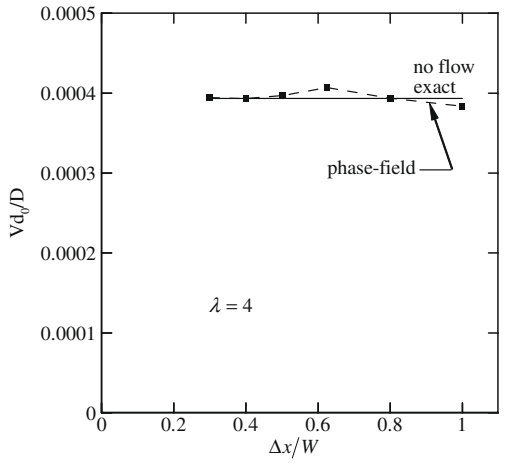

Fig. 3. Convergence of the interface velocity with respect to the grid spacing for growth of a planar gas layer in a supersaturated liquid $\left(Dt/d_0^2 = 20,535\right)$.

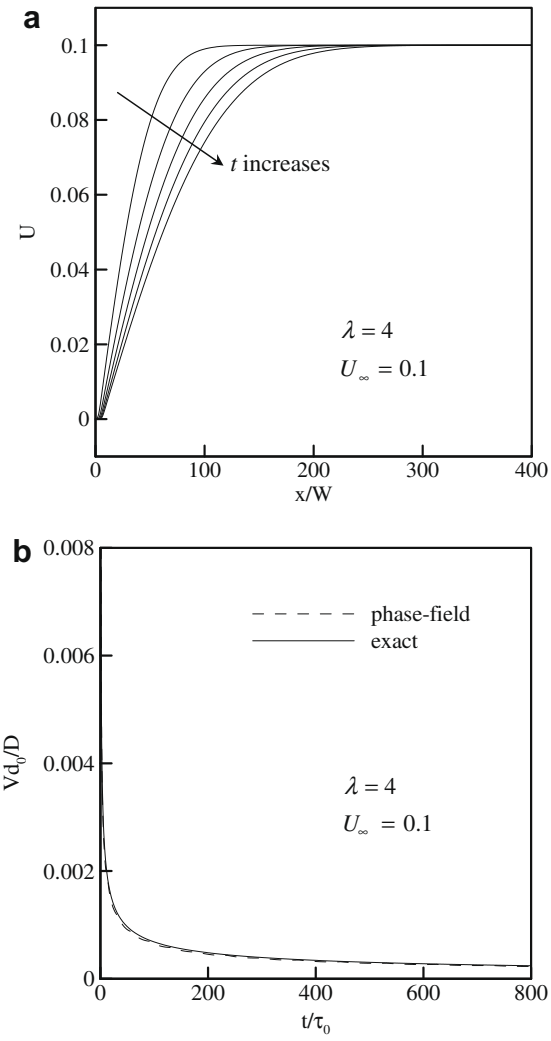

Fig. 4. Phase-field simulation of the growth of a planar gas layer into a supersaturated liquid: (a) evolution of the dimensionless supersaturation profile, every 20,000 time steps; and (b) comparison of the variation of the calculated interface velocity with the exact solution.

evolution of the interface velocity is compared to the exact solution in Fig. 4b. The results match very well and show the expected decrease with square root of time.

3.2. Growth of a spherical bubble

Consider the growth of a single hydrogen bubble into an essentially infinite, supersaturated aluminum melt with an initial hydrogen concentration equal to C_∞, as illustrated in Fig. 5. The system is at a constant and uniform temperature equal to T_0. Initially, a small spherical bubble is assumed to be present at the center of the simulation domain. At the boundaries of the simulation domain, the pressure is fixed at atmospheric pressure (p_{ref}) and the phase-field and concentration field have a zero gradient.

This problem is solved using the full diffuse interface model of Section 2.2 and the parameters and properties in Table 1. Flow is induced during bubble growth due to the large density difference between the gas and the liquid. However, due to the symmetry of the problem, there should be no flow inside of the bubble. Nonetheless, the continuity and momentum equations are solved everywhere, including inside of the bubble. This provides for a check that the velocities in the gas phase are calculated correctly and that there are no spurious currents. The ideal gas law is used to calcu-

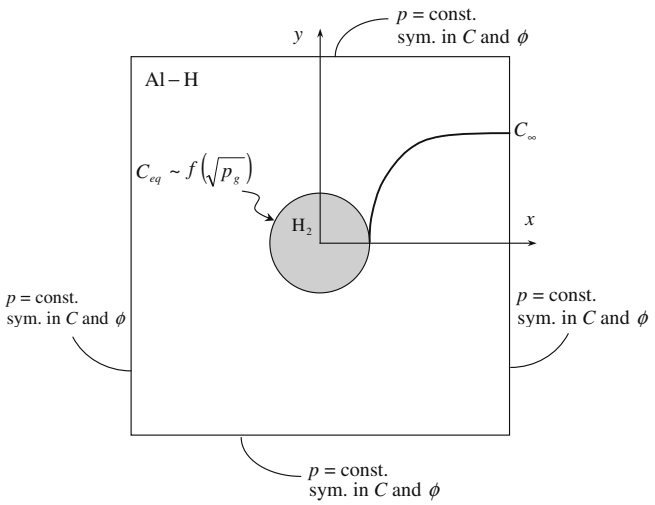

Fig. 5. Growth of a hydrogen bubble in a supersaturated Al–H melt.

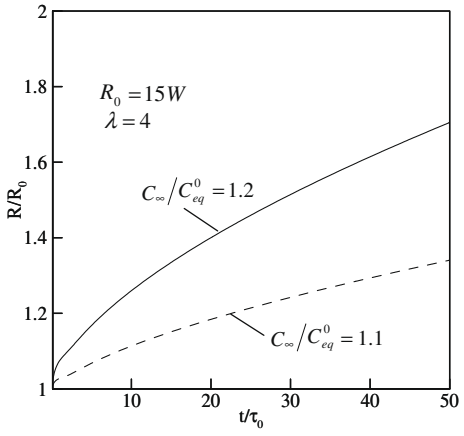

Fig. 6. Predicted evolution of the dimensionless radius of a hydrogen bubble growing into an infinite, supersaturated aluminum melt.

late the gas density as a function of temperature (which is constant at T_0) and the instantaneous gas pressure, p_g. Note that for a stationary, spherical bubble, the gas pressure is uniform, but not constant, because the curvature of the gas–liquid interface decreases as the bubble grows. The initial density ratio in Table 1, r_ρ^0, is obtained by evaluating the gas density at T_0 and p_{ref}.

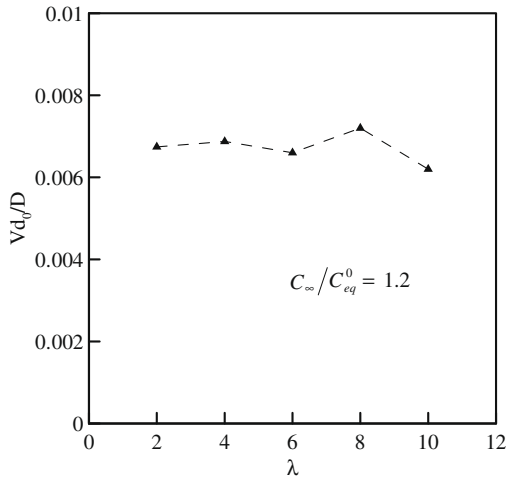

Fig. 8. Convergence of the predicted gas–liquid interface velocity with respect to the diffuse interface coupling constant λ for growth of a hydrogen bubble in a supersaturated aluminum melt ($Dt/d_0^2 = 5134$).

The Hele–Shaw flow equations are solved using a conjugate-gradient pressure Poisson solver on a uniform mesh, as described in Ref. [19]. The phase-field and species equations are solved using an explicit Euler scheme. A fourth-order accurate CENO scheme is used for the advection terms in the phase-field and concentration equations [18]. Numerical tests revealed that it is sufficient to calculate the flow only every 10 time steps of the phase-field and concentration calculations.

Fig. 6 shows the predicted evolution of the bubble radius for two initial supersaturations: $C_\infty/C_{eq}^0 = 1.1$ and 1.2. The simulations give a spherical bubble shape at all times during growth. The radius increases approximately in a square-root-of-time fashion. As expected, the bubble grows faster for a higher initial supersaturation. Fig. 7 shows the calculated velocity vectors and scaled concentration field in the liquid $\left(C_l/C_{eq}^0\right)$ at an intermediate time for the case with $C_\infty/C_{eq}^0 = 1.2$. Due to the density difference between the gas and the liquid, the liquid moves away from the gas–liquid interface as the

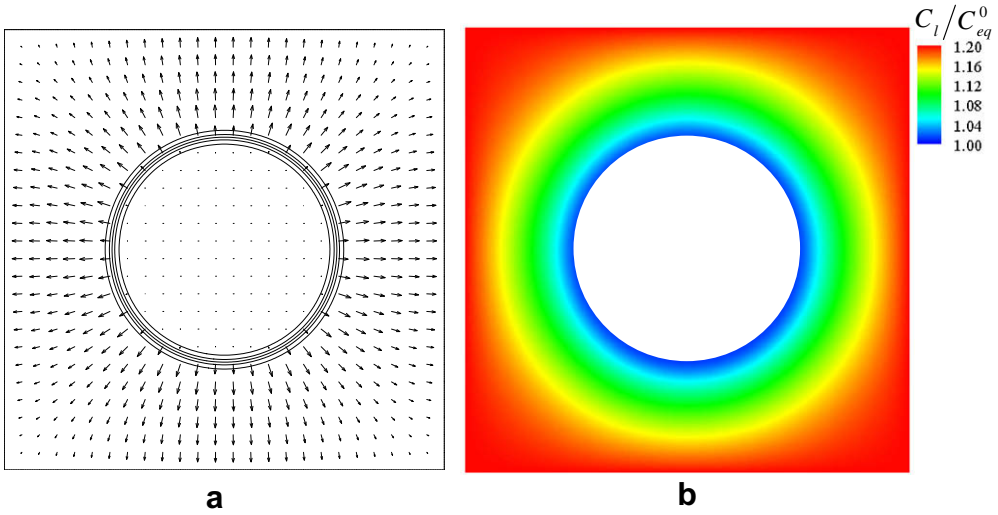

Fig. 7. Predicted dimensionless velocity vectors and phase-field contours (a), and hydrogen concentration field in the liquid (b), for growth of a hydrogen bubble in a supersaturated aluminum melt for $C_\infty = 1.2C_{eq}^0$.

bubble grows and expands (Fig. 7a). The magnitude of the liquid velocity decreases with increasing distance from the gas–liquid interface. No spurious velocities are predicted inside of the bubble. The liquid concentration, C_l, is equal to the equilibrium value, C^0_{eq}, at the gas–liquid interface and increases to the initial concentration, C_∞, for away from the bubble (Fig. 7b). At this time, the concentration boundary layer around the bubble has not yet reached the boundaries of the simulation domain. Its thickness is of the same order as the instantaneous bubble radius.

Fig. 8 demonstrates the convergence of the predicted dimensionless gas–liquid interface velocity, Vd_0/D, with respect to λ $\left(C_\infty/C^0_{eq} = 1.2, Dt/d_0^2 = 5134\right)$. For $\lambda \leqslant 4$, the results converge to a value of $Vd_0/D = 0.0068$. For larger diffuse interface widths, the results become increasingly inaccurate. However, in Fig. 8 the solution does not deteriorate as fast with increasing λ as observed previously in Fig. 2. Nonetheless, a value of $\lambda = 4$ is recommended in a general situation.

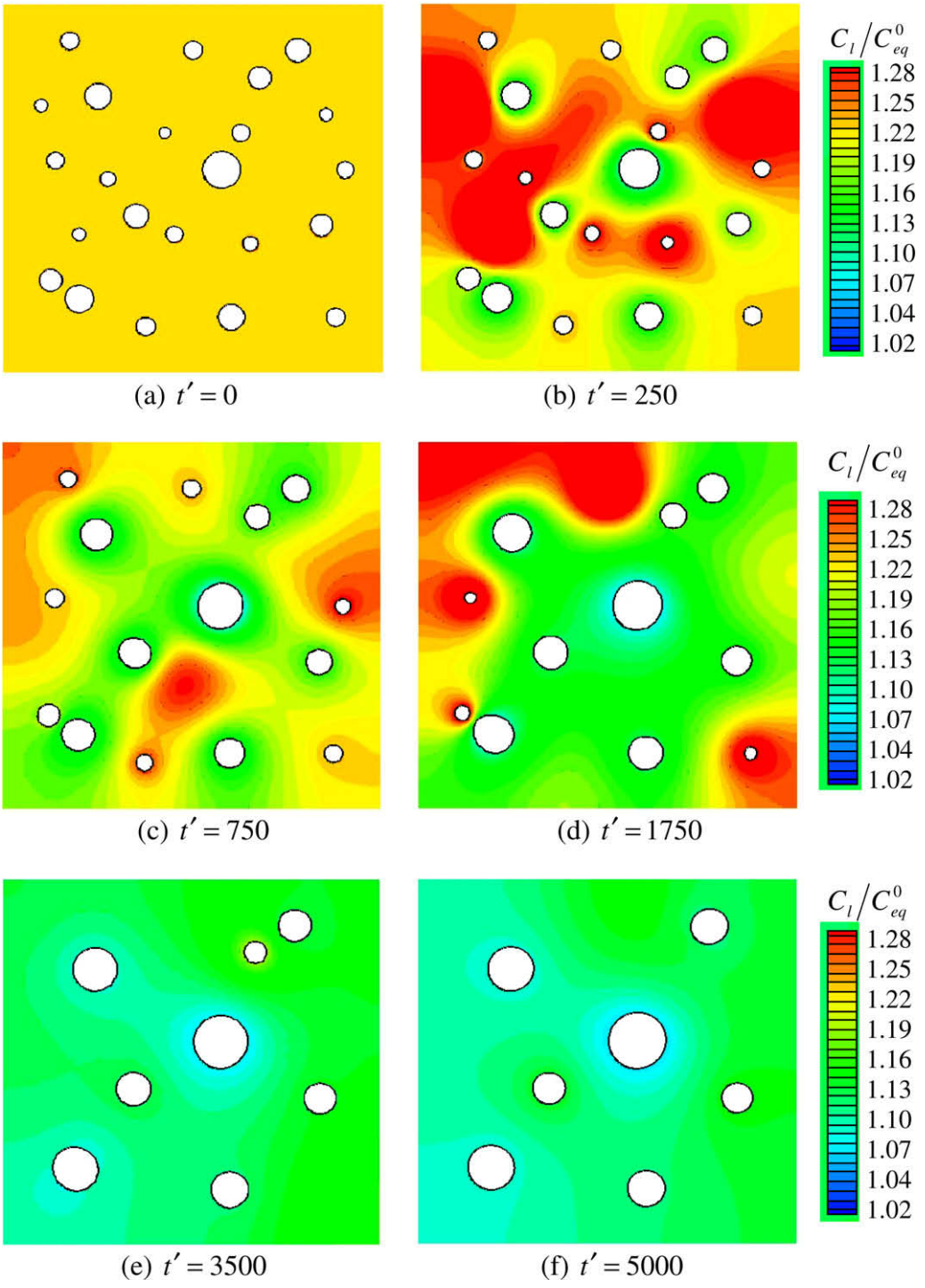

Fig. 9. Simulation of coarsening of hydrogen bubbles in an aluminum melt without flow. The black lines are the $\phi = 0.5$ phase-field contour and the colors indicate the hydrogen concentration in the liquid. The initial gas volume fraction is 5.5%. (For interpretation of the references to color in this figure legend, the reader is referred to the web version of this paper.)

4. Examples

In this section, the diffuse interface model presented in Section 2 is applied to simulate the growth and dynamics of multiple bubbles in a supersaturated liquid inside a Hele–Shaw cell, including bubble coarsening and coalescence, with and without bubble motion. The simulations presented in this section should only be viewed as examples to illustrate some of the capabilities of the present model.

4.1. Bubble coarsening without flow

Coarsening of a dispersion of particles exists in many phase transformation and precipitation processes [27]. The phase-field method has been used to simulate coarsening of a solid–liquid mixture of a binary alloy due to pure diffusion [26,28] and with convection [26]. These studies did not use the thin-interface analysis and the anti-trapping current. In this section, the coarsening of multiple bubbles is simulated using the quantitative phase-field model of Section 2.2.

The present two-dimensional simulation is performed for coarsening of hydrogen bubbles in an isothermal aluminum melt in the absence of flow. As shown in Fig. 9a, the simulation is initialized by randomly placing a number of gas bubbles of different size inside a square domain. The initial bubble volume fraction in the system is equal to 5.5%. The initial hydrogen concentration in the liquid is set to a uniform value of $C_l/C^0_{eq} = 1.2$, which is slightly above the supersaturation due to the initial mean curvature of the bubbles. Thus, there is a small increase in the total bubble volume during coarsening. No-flux conditions are applied on all boundaries of the system.

Fig. 9 shows the predicted evolution of the bubbles with time. The color scale indicates the dimensionless gas concentration in the liquid, C_l/C^0_{eq}. It can be seen that the number of bubbles decreases while the average bubble size increases. The large bubbles grow, while the small ones shrink and eventually disappear. Since the hydrogen concentration in the liquid at the gas–liquid interface is a function of the interface curvature, Eq. (10), the larger (smaller) bubbles have a lower (higher) interfacial hydrogen concentration than the smaller (larger) bubbles. Thus, hydrogen is transported by diffusion through the liquid from the smaller bubbles to the larger bubbles. In other words, the larger bubbles are a sink of hydrogen, whereas the smaller bubbles are a source. This can be clearly seen in Fig. 9 from the species concentration fields around each bubble. At intermediate times, a complex concentration field develops in the liquid. With increasing time, the concentration gradients in the liquid decrease and the coarsening process slows down. Comparing Fig. 9a and Fig. 9f, it can be seen that the average hydrogen concentration in the liquid decreases during coarsening. Due to the low initial bubble volume fraction, no bubble coalescence occurs and the bubbles remain almost spherical. Overall, this simulation demonstrates that the phase-field method easily handles complex interfacial structures and curvature effects.

4.2. Bubble growth and coalescence with and without flow in the gas

Now consider the concurrent growth of two hydrogen bubbles in a supersaturated aluminum melt. Simulations are performed for the same boundary and initial conditions as for the single bubble case discussed in Section 3.2, except that two small bubbles are placed initially near the center of the domain. The initial center-to-center distance between the two bubbles is taken to be equal to $30W$.

In the first set of simulations, the gas velocity is set to zero (by assigning a very large viscosity to the gas phase) and only the liquid is allowed to flow. The assumption of a stationary gas phase is, of course, unphysical, but allows for bubble coalescence to occur. Fig. 10 shows the results of two different simulations: the initial bubbles have the same size, i.e., $R_1 = R_2 = 10W$ (Fig. 10a), and the initial bubble sizes are different, i.e., $R_1 = 7W$ and $R_2 = 14W$ (Fig. 10b). The predicted evolution of the gas–liquid interface is depicted every 2000 time steps. The liquid velocity field is only shown for the last time step. In both cases, the bubbles grow non-spherically, since the hydrogen concentration boundary layers between the two bubbles overlap. Due to diffusion of hydrogen towards both bubbles, the hydrogen concentration in the liquid between the two bubbles quickly reaches values that are lower than elsewhere around the bubbles. Therefore, the growth rate in the region where the two bubbles face each other is reduced and the bubbles take on a deformed shape. Eventually, the two bubbles coalesce. The neck that forms between the two bubbles continues to increase in thickness. Again, these simulations are unphysical, since in reality the flow in the gas phase would quickly equalize the pressure in the bubble after coalescence, but they do demonstrate that interface topology changes are easily handled by the present phase-field method. A simulation with flow in the gas phase is presented below.

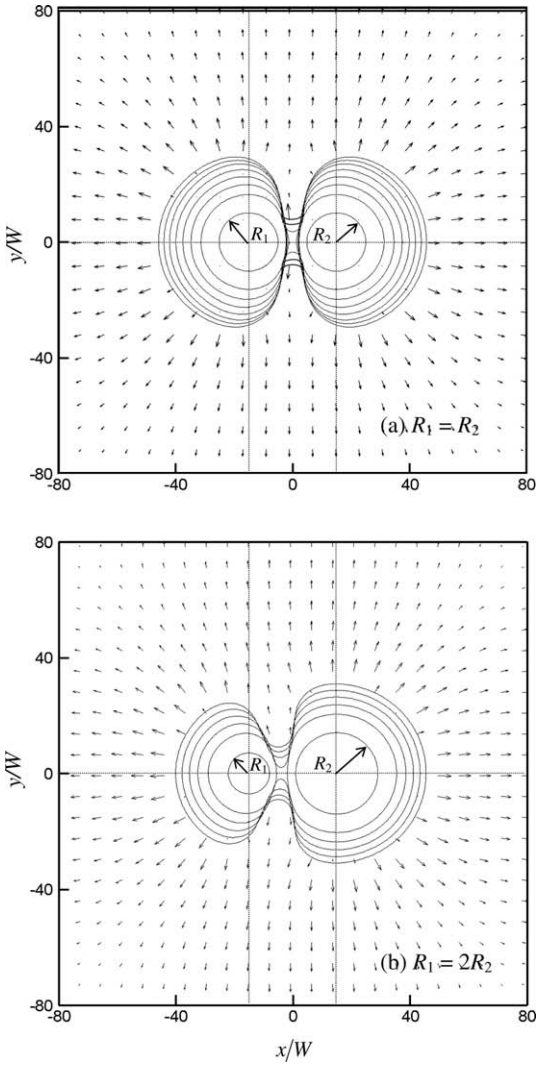

Fig. 10. Simulations of growth of two, closely spaced hydrogen bubbles in a supersaturated aluminum melt without flow in the gas: (a) equal-sized and (b) unequal-sized initial bubbles. The predicted interface contours are shown every 2000 time steps, while the velocity vectors are for the last time step only.

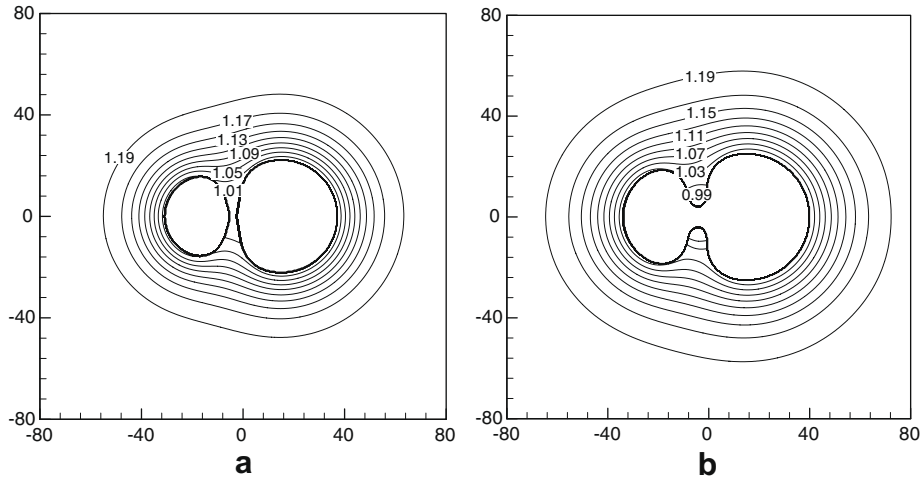

Fig. 11. Predicted dimensionless hydrogen concentration contours for growth of two hydrogen bubbles in a supersaturated aluminum melt: (a) before coalescence and (b) after coalescence.

Fig. 11 shows the predicted hydrogen concentration, C_l/C^0_{eq}, contours in the liquid corresponding to the case of Fig. 10b at two different times: before and shortly after coalescence. Before bubble coalescence (Fig. 11a), the curvature of the gas–liquid interface is positive everywhere. Therefore, the dimensionless hydrogen concentration at the interface, as well as everywhere else in the liquid, is greater than unity. After coalescence (Fig. 11b), the neck between the two bubbles has a negative curvature. Consequently, the dimensionless hydrogen concentration in the liquid near the neck is below unity.

The results of a simulation of the concurrent growth of two bubbles where the flow is calculated in both the liquid and the gas are shown in Fig. 12. This simulation is otherwise identical to the one in Fig. 10a, where the gas is assumed to be stationary. It can be seen that the bubbles remain almost spherical during growth, as opposed to the highly deformed bubble shapes that can be observed in Fig. 10a. This can be explained by the flow inside of a bubble quickly equalizing the gas pressure, such that the equilibrium spherical shape is approached. However, the two bubbles are not stationary inside of the liquid. The two bubbles move away from each other during growth, which can be observed in Fig. 12 by noting that the centers of the (almost spherical) bubbles translate in the x-direction. This effect can be attributed to the expansion flow in the liquid. The expansion flows from the two bubbles meet at the center of the simulation domain, where the velocity is always zero. This creates an asymmetry in the velocity field relative to the center of each bubble, with the majority of the expansion flow being directed away from the center of the simulation domain. By continuity, this flow is not only present in the liquid, but also in the gas phase. Note that inertia and liquid–gas friction effects play no role in Hele–Shaw flows. Due to this movement of the two bubbles away from each other, the bubbles will not coalesce.

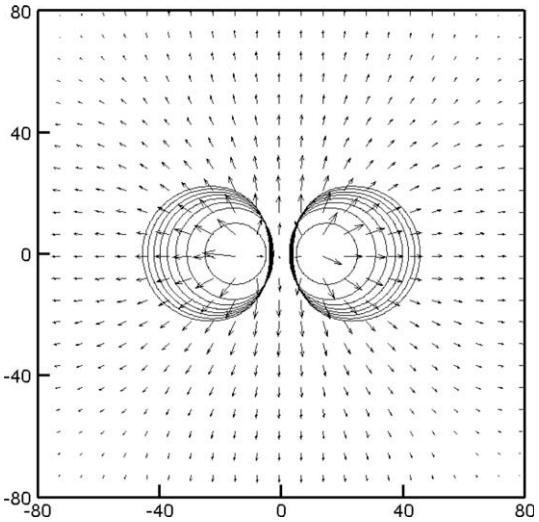

Fig. 12. Simulation of the growth of two equal-sized hydrogen bubbles in an isothermal, supersaturated aluminum melt with flow in the liquid and inside the bubbles. The predicted interface contours are shown every 2000 time steps, while the velocity vectors are for the last time step only.

The above results demonstrate that the present diffuse interface model is well suited for situations that involve bubble growth with interface topology changes, such as bubble coalescence. It also works well for two-phase flows that involve surface tension and large density and viscosity contrasts between the two phases. As reviewed in Section 1, previous modeling studies have not accounted for all of these effects simultaneously.

5. Conclusion

A diffuse interface model has been presented for the simulation of gas bubble growth and flow in a liquid. The model is applied to the hydrogen–aluminum system. The flows in the gas and liquid phases are calculated using a previously developed two-phase model for flows with surface tension, and large density and viscosity differences between the phases [16]. The Hele–Shaw approximation is used to simplify the governing equations for the flow [19]. The phase-field equation models kinetics-free interface motion due to supersaturation of the gas species, curvature, and gas flow. The species conservation equation accounts for advection and diffusion of the gas species in the liquid, and includes an anti-trapping current that is analogous to the one developed for alloy solidification [22,24]. The resulting model converges to the standard sharp interface formulation in the so-called thin-interface limit [22,23], which allows for quantitative numerical simulations to be performed using diffuse interface widths that are of the order of the capillary length (instead of $W \to 0$). The model is validated through a comparison with an available sharp interface solution involving growth of a gas layer in a supersaturated liquid. Convergence of the present model with respect to both the diffuse interface width and the grid spacing is demonstrated for cases involving

a planar and a curved interface. The model capabilities are demonstrated by performing simulations of the coarsening, coalescence, growth and flow of multiple bubbles.

Acknowledgments

This work was supported in part by the US National Science Foundation under Grant No. DMR-0132225.

References

[1] D.C. Venerus, N. Yala, Transport analysis of diffusion-induced bubble growth and collapse in viscous liquids, AIChE J. 43 (1997) 2859–2948.
[2] A. Arefmanesh, S.G. Advani, E.E. Michaelides, An accurate numerical solution for mass diffusion-induced bubble growth in viscous liquids containing limited dissolved gas, Int. J. Heat Mass Transfer 35 (1992) 1711–1722.
[3] H.-Y. Kwak, Y.W. Kim, Homogeneous nucleation and macroscopic growth of gas bubble in organic solutions, Int. J. Heat Mass Transfer 41 (1998) 757–767.
[4] N.G. Lensky, O. Navon, V. Lyakhovsky, Bubble growth during decompression of magma: experimental and theoretical investigation, J. Volcanol. Geoth. Res. 129 (2004) 7–22.
[5] A. Esmaeeli, G. Tryggvason, Direct numerical simulations of bubbly flows. Part 1. Low Reynolds number arrays, J. Fluid Mech. 377 (1998) 313–345.
[6] A. Esmaeeli, G. Tryggvason, Direct numerical simulations of bubbly flows. Part 2. Moderate Reynolds number arrays, J. Fluid Mech. 385 (1999) 325–358.
[7] M. Ohta, S. Haranaka, Y. Yoshida, M. Sussman, Three-dimensional numerical simulations of the motion of a gas bubble rising in viscous liquids, J. Chem. Eng. 37 (2004) 968–975.
[8] M. Ohta, T. Imura, Y. Yoshida, M. Sussman, A computational study of the effect of initial bubble conditions on the motion of a gas bubble rising in viscous liquids, Int. J. Multiph. Flow 31 (2005) 223–237.
[9] D. Jacqmin, Calculation of two-phase Navier–Stokes flows using phase-field modeling, J. Comput. Phys. 155 (1999) 96–127.
[10] H.-G. Lee, J.S. Lowengrub, J. Goodman, Modeling pinchoff and reconnection in a Hele–Shaw cell. I. The models and their calibration, Phys. Fluids 14 (2002) 492–513.
[11] H.-G. Lee, J.S. Lowengrub, J. Goodman, Modeling pinchoff and reconnection in a Hele–Shaw cell. II. Analysis and simulation in the nonlinear regime, Phys. Fluids 14 (2002) 514–545.
[12] R. Folch, J. Casademunt, A. Hernández-Machado, L. Ramírez-Piscina, Phase-field model for Hele–Shaw flows with arbitrary viscosity contrast. I. Theoretical approach, Phys. Rev. E 60 (1999) 1724–1733.
[13] R. Folch, J. Casademunt, A. Hernández-Machado, L. Ramírez-Piscina, Phase-field model for Hele–Shaw flows with arbitrary viscosity contrast. II. Numerical study, Phys. Rev. E 60 (1999) 1734–1740.
[14] D.M. Anderson, G.B. McFadden, A.A. Wheeler, Diffuse-interface methods in fluid mechanics, Annu. Rev. Fluid Mech. 30 (1998) 139–165.
[15] C. Beckermann, H.-J. Diepers, I. Steinbach, A. Karma, X. Tong, Modeling melt convection in phase-field simulations of solidification, J. Comput. Phys. 154 (1999) 468–496.
[16] Y. Sun, C. Beckermann, Diffuse interface modeling of two-phase flows based on averaging: mass and momentum equations, Physica D 198 (2004) 281–308.
[17] D.M. Anderson, G.B. McFadden, A.A. Wheeler, A phase-field model of solidification with convection, Physica D 135 (2000) 175–194.
[18] Y. Sun, C. Beckermann, Sharp interface tracking using the phase-field equation, J. Comput. Phys. 220 (2007) 626–652.
[19] Y. Sun, C. Beckermann, A two-phase diffuse-interface model for Hele–Shaw flows with large property contrasts, Physica D 237 (2008) 3089–3098.
[20] J.W. Tester, M. Modell, Thermodynamics and Its Applications, third ed., Prentice-Hall, Upper Saddle River, NJ, 1996.
[21] R.C. Atwood, S. Sridhar, W. Zhang, P.D. Lee, Diffusion-controlled growth of hydrogen pores in aluminum–silicon castings: in situ observation and modeling, Acta Mater. 48 (2000) 405–417.
[22] A. Karma, Phase-field formulation for quantitative modeling of alloy solidification, Phys. Rev. Lett. 87 (2001) 115701.
[23] A. Karma, W.-J. Rappel, Quantitative phase-field modeling of dendritic growth in two and three dimensions, Phys. Rev. E 57 (1998) 4323–4349.
[24] J.C. Ramirez, C. Beckermann, A. Karma, H.-J. Diepers, Phase-field modeling of binary alloy solidification with coupled heat and solute diffusion, Phys. Rev. E 69 (2004) 051607.
[25] Y.-T. Kim, N. Provatas, N. Goldenfeld, J. Dantzig, Universal dynamics of phase-field models for dendritic growth, Phys. Rev. E 59 (1999) R2546–R2549.
[26] H.-J. Diepers, C. Beckermann, I. Steinbach, Simulation of convection and ripening in a binary alloy mush using the phase-field method, Acta Mater. 47 (1999) 3663–3678.
[27] L. Ratke, C. Beckermann, Concurrent growth and coarsening of spheres, Acta Mater. 49 (2001) 4041–4054.
[28] J.A. Warren, B.T. Murray, Ostwald ripening and coalescence of a binary alloy in two dimensions using a phase-field model, Modell. Simul. Mater. Sci. Eng. 4 (1996) 215–229.